



# The Impact of Solid Dispersion on Formulation, Using Confocal Micro Raman Spectroscopy as Tool to Probe Distribution of Components

M. Elisa Melian<sup>1</sup> · A. Beatriz Munguía<sup>1</sup> · Ricardo Faccio<sup>2</sup> · Santiago Palma<sup>3</sup> · Laura Domínguez<sup>1</sup>

Published online: 16 December 2017

© Springer Science+Business Media, LLC, part of Springer Nature 2017

## Abstract

**Purpose** Solid dispersions (SDs) of a poorly water-soluble drug were prepared, and their physicochemical properties were compared to those of control physical mixtures (PMs). Among the multiple techniques used to characterize the solid state of preparations, confocal micro Raman spectroscopy (CMRS) was used as a non-destructive tool to qualitatively probe content uniformity and distribution of drug and carrier.

**Methods** SDs and PMs of drug (fenbendazole, FBZ) were prepared containing two different carriers (poloxamer P188 or P407) with different drug polymer ratios. The preparations were characterized by powder X-ray diffractometry, Fourier transform infrared spectroscopy, thermal analysis, scanning electron microscopy, and in vitro dissolution assay. In addition, CMRS technique and principal component analysis (PCA) were used in order to statistically define the content uniformity and distribution of the drug within the polymeric matrix.

**Results** In vitro dissolution results exhibited a marked improvement when the drug was formulated as SD compared to control PM and to pure drug. The solid state of these preparations characterized by X-ray powder diffraction and Fourier transform infrared spectroscopy showed no changes in the crystalline state of the drug and no chemical interactions between the components. Raman studies showed a better content uniformity of the drug within the polymeric matrix when subjected to SD process, correlating with the improved dissolution profile.

**Conclusion** This study provides evidence of the potential of the confocal Raman imaging technique, providing a fast and powerful method to characterize solid dispersions which could be incorporated towards the use of quality by design (QbD) approaches in pharmaceutical development.

**Keywords** Confocal micro Raman spectroscopy · Content uniformity · Solid dispersion · Dissolution rate

**Electronic supplementary material** The online version of this article (<https://doi.org/10.1007/s12247-017-9306-9>) contains supplementary material, which is available to authorized users.

✉ Laura Domínguez  
ldoming@fq.edu.uy

<sup>1</sup> Área de Farmacología, Depto. CIENFAR, Facultad de Química, Universidad de la República (Udelar), Av. General Flores 2124, Montevideo, Uruguay

<sup>2</sup> Centro NanoMat & Cryssmat-Lab, DETEMA, Facultad de Química, Universidad de la República (Udelar), Av. General Flores 2124, Montevideo, Uruguay

<sup>3</sup> Unidad de Investigación y Desarrollo en Tecnología Farmacéutica, UNITEFA (UNC-CONICET), Depto. de Farmacia, Facultad de Ciencias Químicas, Universidad Nacional de Córdoba (UNC), Haya de la Torre y Medina Allende, Ciudad Universitaria, Córdoba, Argentina

## Introduction

The majority of failures in new drug development are associated with poor water solubility that can lead to low bioavailability, resulting in suboptimal drug delivery. This fact is critical to oral administration, the most economic and convenient route, in which the absorption of drugs in the gastrointestinal tract depends mainly on their solubility and permeability properties. From an estimated 40% of approved drugs, around 90% are poorly soluble molecules, therefore, advances in different insoluble drug delivery technologies are attractive alternatives, including for reformulate marketed drugs to improve efficacy (which may be of interest for the pharmaceutical industry as it provides clinical and economic benefits) [1]. Many techniques have been developed to improve drug solubility and dissolution rate of drugs with

poor water solubility as polymorphs, the amorphous form of the drug, complexation, decreasing particle size of the drug by milling, salt formation, liposomes, solid dispersions, etc. [2]. In particular, solid dispersions (SDs) consist of mixtures of poorly water-soluble drugs in hydrophilic carriers which, depending on their properties, drive the drug release profile [3, 4]. Different processes for the manufacturing of SDs are described as solvent and fusion methods, spray drying, coprecipitation, co-evaporation, and freeze drying techniques. Among melting methods, low temperature fusion is an alternative when the API or carrier is not thermostable at high temperature [5]. This modified technique consists in suspending the API in a previously molten carrier, instead of heating both drug and carrier at the same time. This allows reducing heating time and process temperature [5]. This manufacturing process is a simple and environmentally friendly non-solvent technology which is cost-effective and can be easily scaled up for commercial purposes [6, 7].

Dissolution enhancement of poorly water-soluble drugs in solid dispersions can be assessed by standard dissolution tests. In addition, other properties of SDs as physical state of the drug, the drug-carrier interaction, the content uniformity and distribution of components, among others must be studied to characterize pharmaceuticals [5]. What is more, the use of quality by design (QbD) approaches considers quality associated into a product than testing for acceptability after production, based on the processes understood thoroughly, a concept to be introduced in the pharmaceutical industry [8]. In this sense, many instrumental techniques are applied to measure these properties, as powder X-ray diffraction (PXRD) and differential scanning calorimetry (DSC) to determine the crystalline state of drug; Fourier transformed infrared (FTIR) spectroscopy and thermal gravimetry analysis (TGA) to investigate chemical stability and molecular interaction; scanning electron microscopy or atomic force microscopy to qualitatively characterize the morphology of SDs, among others [9].

In this sense, the use of chemical imaging methods combining microscopy and spectroscopy allows us to know spatial properties of a particular compound into complex systems in a non-destructive way, not available otherwise. Particularly, Raman spectroscopy has been proved to be a useful tool for identification and characterization of solid state properties of pharmaceuticals, including SD studies [10–13]. It is a robust and reliable method with a low limit of detection and minimal sample preparation, with renewed interest of application in pharmaceutical development to characterize among others, content uniformity (composition, distribution, etc.) and chemical aspects as stability [14].

Additionally, the utilization of statistical tools, like PCA, implemented to the confocal Raman imaging technique provides a powerful and fast methodology for the data analysis and the conclusions than can be drawn [15].

Fenbendazole (FBZ) was used in this work, as a model drug belonging to the important class of broad-spectrum benzimidazole (BZ) anthelmintics, worldwide used for the prevention and treatment of parasitic diseases, in veterinary and human medicine, despite their low bioavailability that is hindered by its low aqueous solubility [16]. Nevertheless, the need for new anthelmintic drugs is a concern both for anthelmintic resistance against commercially available drugs for a variety of nematodes of veterinary importance and for several parasites of humans [17, 18]. In this sense, and as part of an ongoing research project to search for new anthelmintics, we have communicated a series of novel valerolactam-benzimidazole hybrids [19, 20] that showed low solubility, similar to their commercial benzimidazole precursors. Then, even when the need to develop new anthelmintic drugs is indisputable, they must be conveniently formulated in order to maximize their availability and efficacy. Similarly, we must also consider the enormous potential for improving existing drugs that are still efficacious by modification of their formulation/delivery, in order to use existing actives more effectively [21].

In this work, solid dispersions of a poorly soluble drug (FBZ) were prepared by a low-temperature fusion method, using two different types of oral safe carriers, poloxamers (polyoxyethylene-polypropylene block copolymer non-ionic surfactants) P407 and P188 [22–24]. The formulations were characterized in terms of solid state properties among others, and chemical imaging was explored as a fast, powerful, and non-destructive tool to characterize the content uniformity and distribution of components of solid dispersions (SDs).

## Materials and Methods

### Chemicals

Fenbendazole (FBZ, pharmaceutical grade) was kindly donated by Laboratorio Uruguay S.A. (LUSA, Montevideo, Uruguay). Poloxamer 188 (P188) and poloxamer 407 (P407) were provided by BASF (Ludwigshafen, Germany). All other reagents were of analytical grade.

### Preparation of Solid Dispersions

FBZ SDs were prepared by dispersing FBZ in melted P188 or P407 at different ratios (Table 1) in a water bath at 65 °C. The mixtures were homogenized by stirring. The resulting homogeneous preparations were rapidly cooled and pulverized. The formulations were sieved to obtain a maximum particle size of 250 µm and stored in screw-capped glass vials at 8 °C.

Control physical mixtures (PMs) of FBZ and poloxamer were prepared in order to compare the SDs against the simple mixture of its components. PMs were prepared by manually mixing the appropriate amount of FBZ and carrier previously

**Table 1** Solid dispersions and physical mixtures composition

SD	PM	FBZ (wt.%)	P188 (wt.%)	SD	PM	FBZ (wt.%)	P407 (wt.%)
SD11	PM11	5	95	SD21	PM21	5	95
SD12	PM12	10	90	SD22	PM22	10	90
SD13	PM13	25	75	SD23	PM23	25	75
SD14	PM14	50	50	SD24	PM24	50	50

pulverized and sieved to a maximum particle size of 250  $\mu\text{m}$  (composition detailed in Table 1).

### FBZ Solubility and Dissolution Assay

Excess amounts of pure FBZ were added to 5 mL of HCl 0.1 N in hermetic tubes (by triplicate) transferred to a thermostatic bath (Vicking Dubnoff, Argentina) at 37 °C. After 48 h, 1 mL of suspension was withdrawn and filtered through a Millipore 0.45- $\mu\text{m}$  membrane filter and quantified by UV-visible spectrophotometry (Thermo Evolution 300). Measurements were performed at 298.5 nm. The calibration curve of the drug follows linearity in the concentration range from 1.6 to 10.0  $\mu\text{g/mL}$ , with a correlation coefficient value of 0.995 and a limit of quantification (LOQ) for FBZ of 0.23  $\mu\text{g/mL}$ .

In vitro drug release studies of powered FBZ, SDs, and PMs (equivalent to 5 mg of FBZ, SINK conditions) were performed using USP dissolution apparatus 2 (SR6 SR11-6-Flask Dissolution Test Station, Hanson Research), adapted with 0.45- $\mu\text{m}$  filters for sampling, at a paddle rotation speed of 50 rpm in 900 mL of HCl 0.1 N, at 37.0 °C. Filtered samples were collected at 3, 5, 10, 15, 30, and 60 min and assayed for fenbendazole content by UV-visible spectrophotometry at 289.5 nm. The profiles were statistically compared using a model independent approach by calculating the difference factor (F1) and

similarity factor (F2) among the profiles as described in bibliography [25].

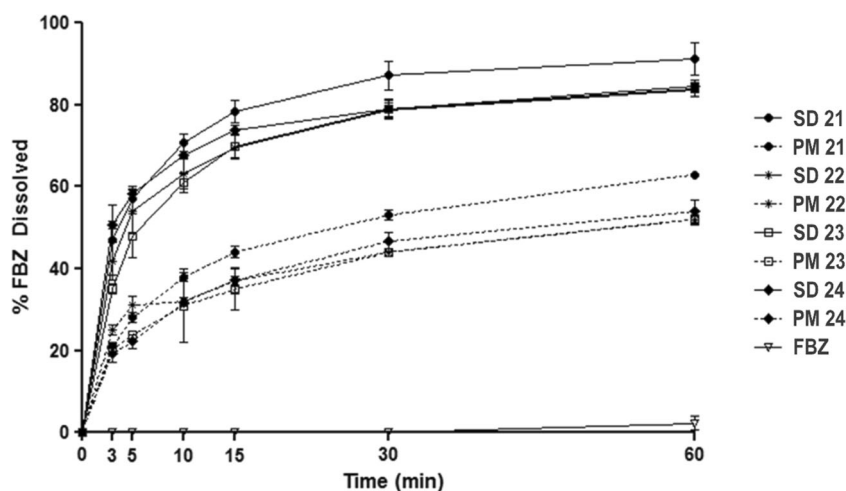
### Physical-Mechanical Properties: Density, Compressibility, and Angle of Repose

The density of the samples was determined by gently pouring the powder into a 10  $\text{cm}^3$  graduated cylinder. The bulk density (BD) was calculated as the ratio between weight (g) and volume ( $\text{cm}^3$ ). To determine the tap density (TD), the cylinder was tapped in vertical drop until no measurable change in volume was noticed. The Hausner ratio (HR) and the Carr's Index (CI) were calculated in order to evaluate the compressibility of the powder. The angle of repose ( $\alpha$ ) for each mixture of powders was determined by the funnel method [26].

### Thermal Analysis

Thermogravimetric analysis (TGA) and differential scanning calorimetry (DSC) curves were obtained using a Jupiter STA 449, Netzch simultaneous thermal analysis equipment. A sample of around 5 mg was placed in sealed aluminum crucibles with pierced lids. Measurements were made from 27 up to 500 °C using a heating rate of 10 °C/min. The sensors and the crucibles were under a constant flow of nitrogen (70 mL/min) during the experiment. The fusion and decomposition

**Fig. 1** Dissolution profiles of SDs and PMs containing P407, see the “FBZ solubility and dissolution assay” section for experimental details



temperatures were taken as the extrapolated onset temperature of the endothermic/exothermic peak.

### Fourier Transform Infrared Spectroscopy

Fourier transform infrared (FTIR) spectroscopy was performed using FTIR spectrometer IR-Prestige 21 (Shimadzu, Japan). The formulations were characterized using KBr disks from 4000 to 500  $\text{cm}^{-1}$ , at a resolution of 2  $\text{cm}^{-1}$ .

### X-ray Powder Diffraction

X-ray powder diffraction (XRPD) was performed using a Rigaku Ultima IV diffractometer operating in a Bragg-Brentano geometry, with  $\text{CuK}\alpha$  radiation measuring the  $2\theta = 4.00\text{--}60.00^\circ$  range using  $2\theta$  steps of  $0.02^\circ$  with a 10-s integration time per step. In order to estimate changes in the crystallinity of drug and carrier, XRPD studies with internal standard (IS) using  $\text{Y}_2\text{O}_3$  (yttrium oxide) were carried out. For this purpose, we mixed a 20% weight to weight of  $\text{Y}_2\text{O}_3$  with the SD and PM formulations. Every diffraction peak of FBZ and P407 was normalized by the corresponding areas, in reference to the internal standard peaks. Once normalized, the peak areas of FBZ and P407 in the SD were compared with the corresponding peaks in the PM. FBZ and poloxamer crystallinity after the SD procedure were calculated considering the PM components as the initial crystalline state (100%).

### Confocal Raman Microscopy

Confocal Raman spectroscopy was performed using a WITec Alpha 300-RA confocal Raman spectrometer equipment. The excitation laser wavelength corresponds to  $\lambda = 532$  nm, and the power was adjusted to 45 mW to avoid sample decomposition. Raman spectra were obtained by averaging a set of 22,500 spectra with 0.053-s integration time for each spectrum. The spectrometer operating with a grating of 600 lines/mm allowed us to obtain a resolution of  $\sim 4$   $\text{cm}^{-1}$  in the range of 70 to 4000  $\text{cm}^{-1}$ . All the images were collected at the resolution optical limit of 300 nm.

Principal component analysis (PCA) and peak to peak intensity ratio normalization, adapted from Karavas et al. [10], were used for probing the spatial distribution of FBZ in the samples.

### Scanning Electron Microscopy

Particle morphology, size, and shape characteristics of pure FBZ, pure P188, SDs, and PMs were examined using a scanning electron microscope (ZEISS, Sigma, Germany). Samples were attached to an adhesive conducting tape mounted on the SEM stubs and were coated with Au before examination.

**Table 2** Percentage of FBZ dissolved for each formulation within 15 min of the dissolution assay expressed as mean and standard deviation. NQ indicates detected but not quantifiable

% FBZ dissolved (mean $\pm$ SD)			
SD	15 min	PM	15 min
SD11	74.8 $\pm$ 3.2	PM11	41.9 $\pm$ 1.4
SD12	68.4 $\pm$ 1.2	PM12	38.1 $\pm$ 3.1
SD13	72.4 $\pm$ 0.8	PM13	39.4 $\pm$ 1.5
SD14	71.9 $\pm$ 1.4	PM14	44.4 $\pm$ 1.4
SD21	78.4 $\pm$ 2.4	PM21	44.7 $\pm$ 1.4
SD22	69.7 $\pm$ 3.0	PM22	37.2 $\pm$ 1.2
SD23	70.5 $\pm$ 2.9	PM23	35.0 $\pm$ 0.5
SD24	73.9 $\pm$ 0.1	PM24	37.1 $\pm$ 3.2
FBZ	NQ		

## Results and Discussion

### Dissolution Assays

According to FBZ solubility assay (31.3 mg/L at 48 h, HCl 0.1 N, 37  $^\circ\text{C}$ ), we determined the amount of FBZ to be used in the dissolution study following SINK conditions. FBZ dissolution profiles of pure FBZ, SDs, and PMs containing P407 are shown in Fig. 1. All SDs showed improved dissolution rate of FBZ, compared to the corresponding control PMs (Online Resource 1), demonstrating the utility of SD procedure. The approach used to compare the dissolution profile of each SD with its corresponding PM indicated that the curves of SDs and PMs of equal composition were not similar (Online Resource 2). In fact, within the first 15 min of the dissolution assay, the amounts of FBZ dissolved from SDs doubled those of the PMs (Table 2) both for P188 and for P407. Nevertheless, the dissolution profiles of all SDs were

**Table 3** Physical-mechanical properties of formulations containing 95 and 50 wt.% of P407, pure FBZ, and pure P407

Physical-mechanical properties				
	P407 wt.%	Angle of repose ( $\alpha^\circ$ )*	Carr's Index (CI)*	Hausner ratio (HR)*
SD21	95	22.7	27.7	1.4
PM21	95	21.2	25.9	1.3
SD24	50	22.1	26.8	1.4
PM24	50	46.6	46.4	1.8
FEB	0	47.4	48.8	1.9
P407	100	19.5	29.8	1.4

\*See the “Physical-Mechanical Properties” section for experimental details

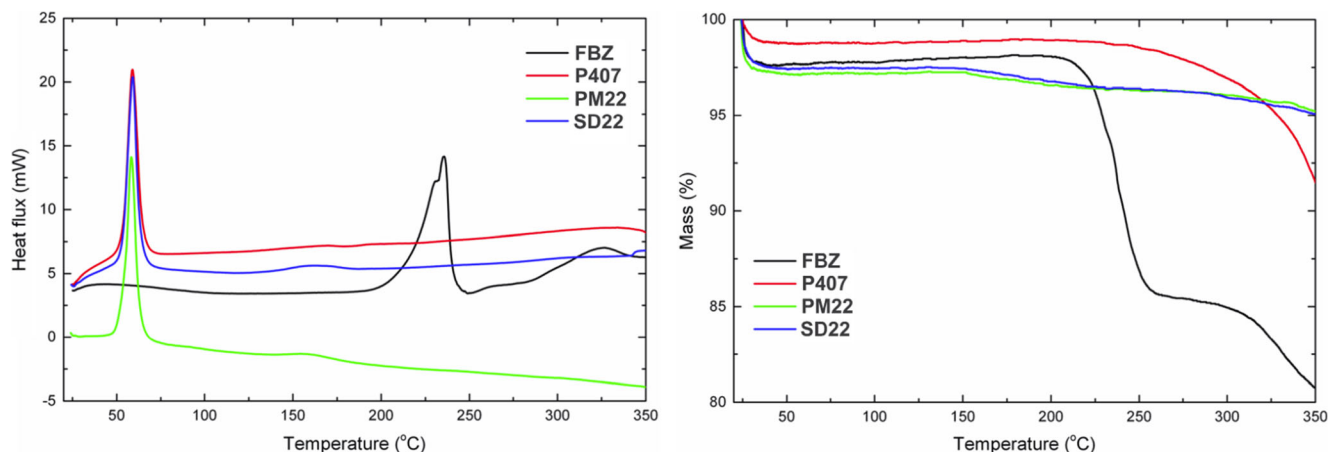


**Fig. 2** DSC and TGA thermograms of SD22, PM22, FBZ, and P407

similar according to  $d_e F_1$  and  $F_2$  calculated values, indicating that the different carriers and the drug/carrier ratio did not affect the release of the drug (Online Resource 2).

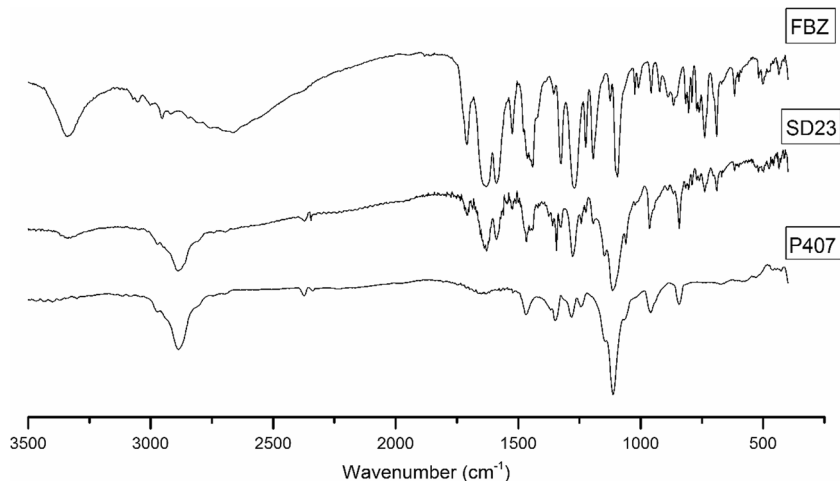
In previous works, we explored the use of poloxamer as a carrier for preparing solid dispersions of albendazole (ABZ) [27]. In that case, it was observed that the relative ratio of the components (drug/carrier) was a key factor. SDs with lower P188 percentage (50, 75 wt.%) seemed to be more effective in increasing ABZ dissolution rate. A possible explanation of these results could be that this type of polymers can form thermoreversible gels. However, no differences between the proportions explored were found in this study. This could be attributed to differences in drug solubility (FBZ 0.01 mg/L; ABZ 10 mg/L, H<sub>2</sub>O, 25 °C) [28]. When DSs are dispersed in water, carriers often dissolve or disperse rapidly due to their hydrophilic property and form a concentrated layer or a gel layer in some cases. If the drug is insoluble or sparingly soluble in the concentrated layer, it can be released intact to contact with water and the dissolution

profile depends on the properties of the drug particles (polymorphic state, particle size, drug solubility) [29]. In this sense, we hypothesize that ABZ dissolution is governed by the carrier's properties, while for FBZ, the drug which plays a central role given its lower solubility could explain why there are no significant differences regarding the concentration of polymer used. In addition, the significantly increased dissolution rate of FBZ when poloxamers are used as carriers may be attributed to its wettability, emulsification, and solubilization effects.

### Physical-Mechanical Properties

Flow and compressibility parameters were studied as important physical-mechanical properties for the preparations of oral dosage forms. The results of the measured angle of repose, Carr's Index, and Hausner ratio of SDs and PMs, particularly those containing 95 and 50 wt.% of FBZ, are shown in Table 3. Compared to FBZ, all preparations showed improved rheological properties

**Fig. 3** FTIR spectrum of pure FBZ, pure P407, and SD23 containing both compounds



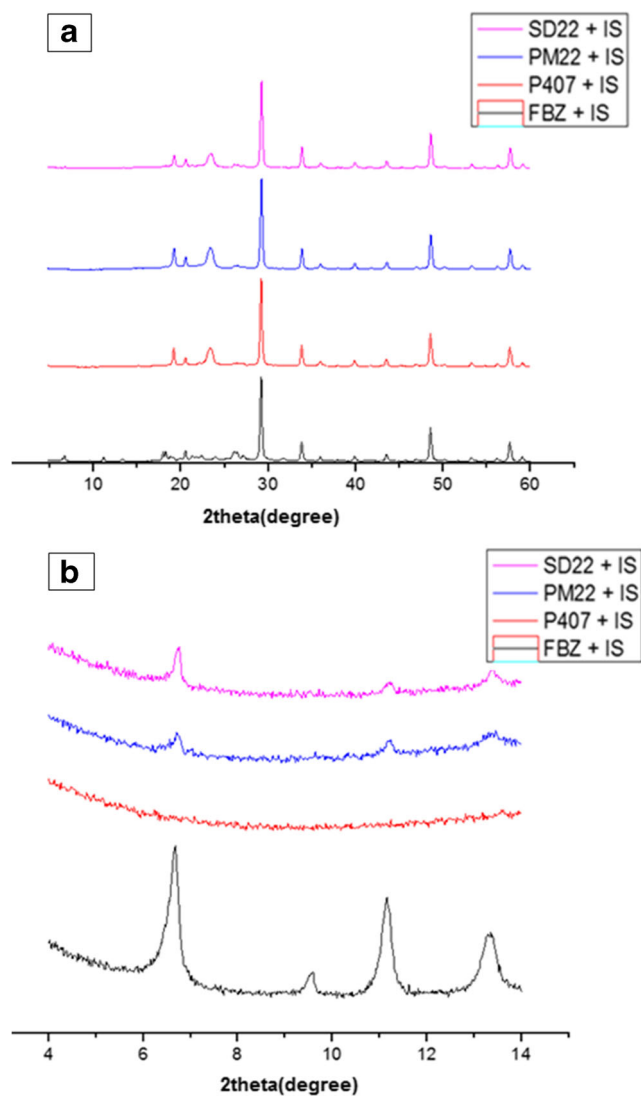


**Fig. 4** **a** XRPD diffractograms with  $Y_2O_3$  as internal standard. From bottom to top: FBZ, P407, PM22, SD22. **b** XRPD diffractograms with  $Y_2O_3$  as internal standard, amplification of the FBZ peaks zone. From bottom to top: FBZ, P407, PM22, SD22

(Online Resource 3) and all SDs showed excellent flow properties [26], particularly compared with the PMs, which could be attributed to the more homogeneous distribution of FBZ within the SDs (see the “Confocal Raman Microscopy” section).

## Physicochemical and Structural Characterization

### Thermal Analysis

DSC and TGA results showed that FBZ melts with decomposition at 210 °C (Fig. 2). DSC results confirmed the reduction in crystallinity observed in XRPD experiments since poloxamer-normalized melting endotherm showed a

10% reduction in terms of enthalpy ( $\Delta H_{mel}$ ) when incorporated in SD22 as regards to the PM22.

### FTIR and XRPD

From the more relevant infrared signals corresponding to pure FBZ (3336.12; 1630.31; 742.28; 685.11  $cm^{-1}$ ) and P188 or P407 (2881.43; 1281.52; 1117.75  $cm^{-1}$ ), those that were exclusive signals of each component remain clearly unaltered in the SDs and PMs collected spectra suggesting the absence of chemical interactions between the components in the different formulations (Fig. 3). This observation was confirmed by XRPD where the diffractograms of SDs and PMs showed the signals assigned to each pure component unchanged (FBZ  $2\theta(^{\circ}) = 6.68, 11.16, 13.36$ ; P407:  $2\theta(^{\circ}) = 19.18, 23.36$ ) (Fig. 4).

In fact, XRPD studies using  $Y_2O_3$  as an internal standard (100% crystalline, main signals  $2\theta(^{\circ}) = 29.45; 34.05; 48.57$ ) were conducted to estimate crystalline fractions of carrier and drug in the different preparations. Previous experiments suggested that the SD process of manufacturing did not affect FBZ crystallinity, although a slight change was detected in poloxamer crystalline fraction. It is important to mention that we selected diffraction peaks of FBZ, P188/P407, and  $Y_2O_3$ , which do not appreciably overlap as observed from the diffractograms of the three pure components (Fig. 4a). The results confirmed that there were not any significant differences neither of the crystalline structure nor the crystalline fraction of the drug FBZ when it was formulated as SD or PM (Fig. 4b). Nevertheless, a crystallinity reduction of around 30% for P407 was observed in the SD22 in comparison to PM22 (Table 4), suggesting that the SD procedure affected the crystalline order of the carrier fraction with almost no change in the FBZ phase fraction.

### SEM

SEM images of FBZ showed an irregular flat-shaped crystalline solid with a distribution size of 5–20  $\mu m$  and a smooth surface (Fig. 5a), while the carrier micrographs showed a

**Table 4** Crystalline fraction comparison of SD components with respect to the PM

FBZ		P407	
Peak position (degree)	SD crystalline fraction <sup>a</sup>	Peak position (degree)	SD crystalline fraction <sup>a</sup>
6.60	117.0	19.30	68.3
11.20	96.2	23.20	73.8
13.40	94.9		
Mean $\pm$ SD	102.7 $\pm$ 11.2	Mean $\pm$ SD	71.0 $\pm$ 3.7

<sup>a</sup> Expressed as percentage (see the “X-ray powder diffraction” section for experimental details)

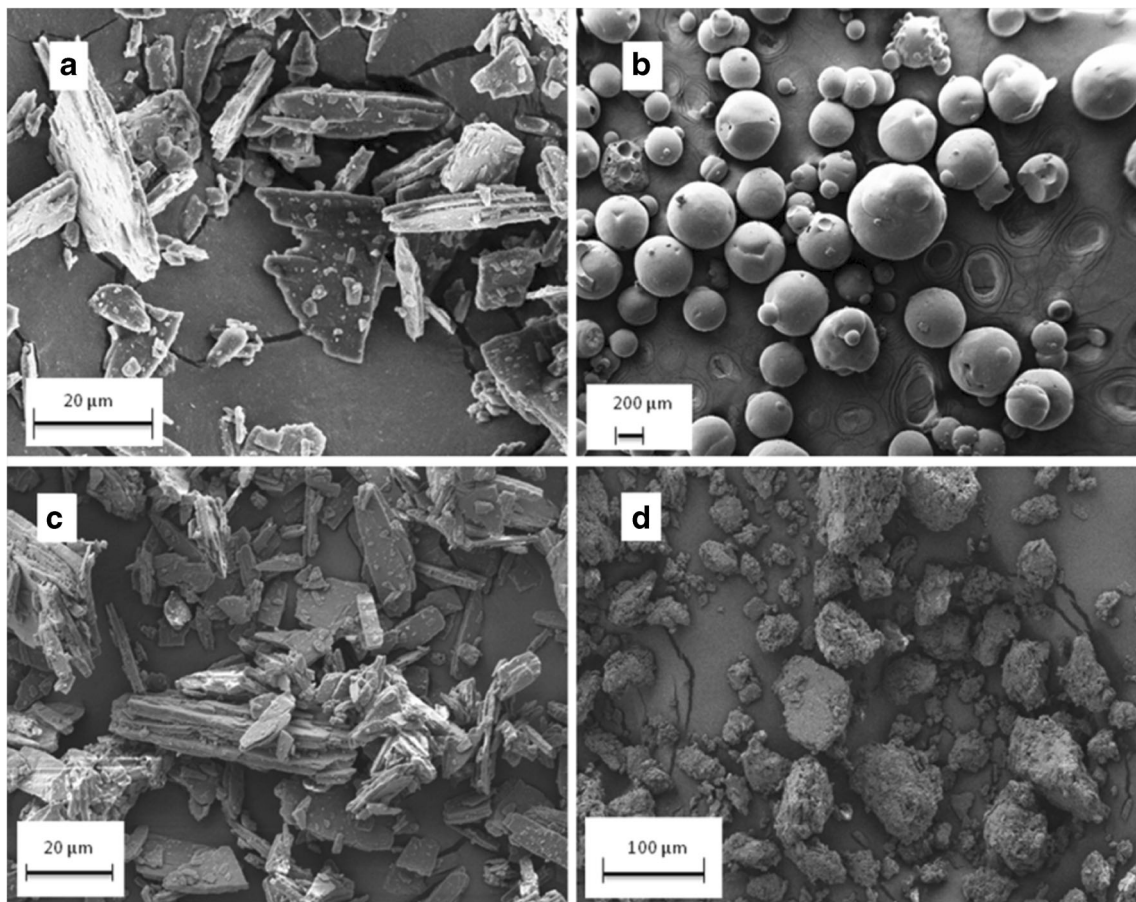


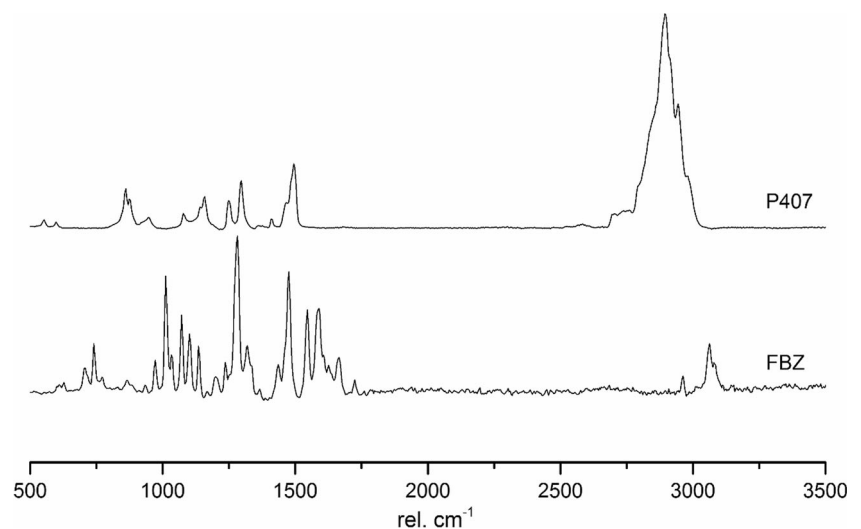
**Fig. 5** SEM micrographs of **a** FBZ 2.34KX, **b** P188 24X, **c** MF14 745X, **d** SD14 104X

smooth surface spherical particles of 200–500 µm (Fig. 5b). On the other hand, the solid dispersion (SD14) and physical mixture (PM14) (1:1 FBZ:P407) showed a clearly different appearance. In fact, while PM images showed acicular and flat particles (Fig. 5c), those of the SD were rounder and homogeneous (Fig. 5d).

### Confocal Raman Microscopy

Raman spectra of pure FBZ and P407 were collected (Fig. 6). The 2-dimensional (2D) confocal Raman microscopy images were obtained by getting single Raman spectra for every single pixel of the selected images. This procedure was performed on

**Fig. 6** Raman spectra of FBZ (below) and P407 (above)



SD22 and PM22 samples (FBZ 10 wt.%) at random locations in areas of  $15 \times 15 \mu\text{m}^2$ , with a grid of  $85 \times 85$  points defining the bitmap image. The mapping results were normalized in terms of peak intensity ratios in order to avoid point-to-point variations produced by height differences on the sample surface [10]. The collected Raman spectra of crystalline FBZ and P407 are shown in Fig. 7. The selected signals were  $1591 \text{ cm}^{-1}$  for FBZ and  $866 \text{ cm}^{-1}$  for P407, and the ratio was calculated as  $I_{1591}/I_{866}$ . These peaks were exclusive signals of each component and no interferences with other signals were detected at their wavelength (Fig. 6). We proceeded with scripts prepared in our group in order to obtain the histograms of the different intensity ratio distributions, and presented as complementary statistical information [30].

The SD mapping showed better content uniformity and distribution of FBZ in comparison to the PM, although a FBZ concentrated spot of  $2\text{--}3 \mu\text{m}$  was detected (Fig. 7a).

The PM mapping showed four spots of concentrated FBZ, with a mean size of  $4 \mu\text{m}$  without any other signal indicating FBZ distribution within the polymer matrix, demonstrating poor homogeneity and blending between the active and the matrix (Fig. 7b). Histograms showing the distribution of the calculated ratios and their density in the image are also shown in Fig. 7, on the right of their corresponding 2D mapping. These charts correlate very well with the information given by the images. In fact, the histogram corresponding to the SD shows a less discrete distribution than the distribution of PM and a more homogeneous density. On the other hand, the PM histogram shows just a few ratio bars, and high-density values compared to the SD. This difference would indicate an SD image formed by pixels including a wide range of combinations of FBZ/P407 ratios, as opposed to a PM image formed by pixels where either FBZ or P407 spectra domains presented signals.

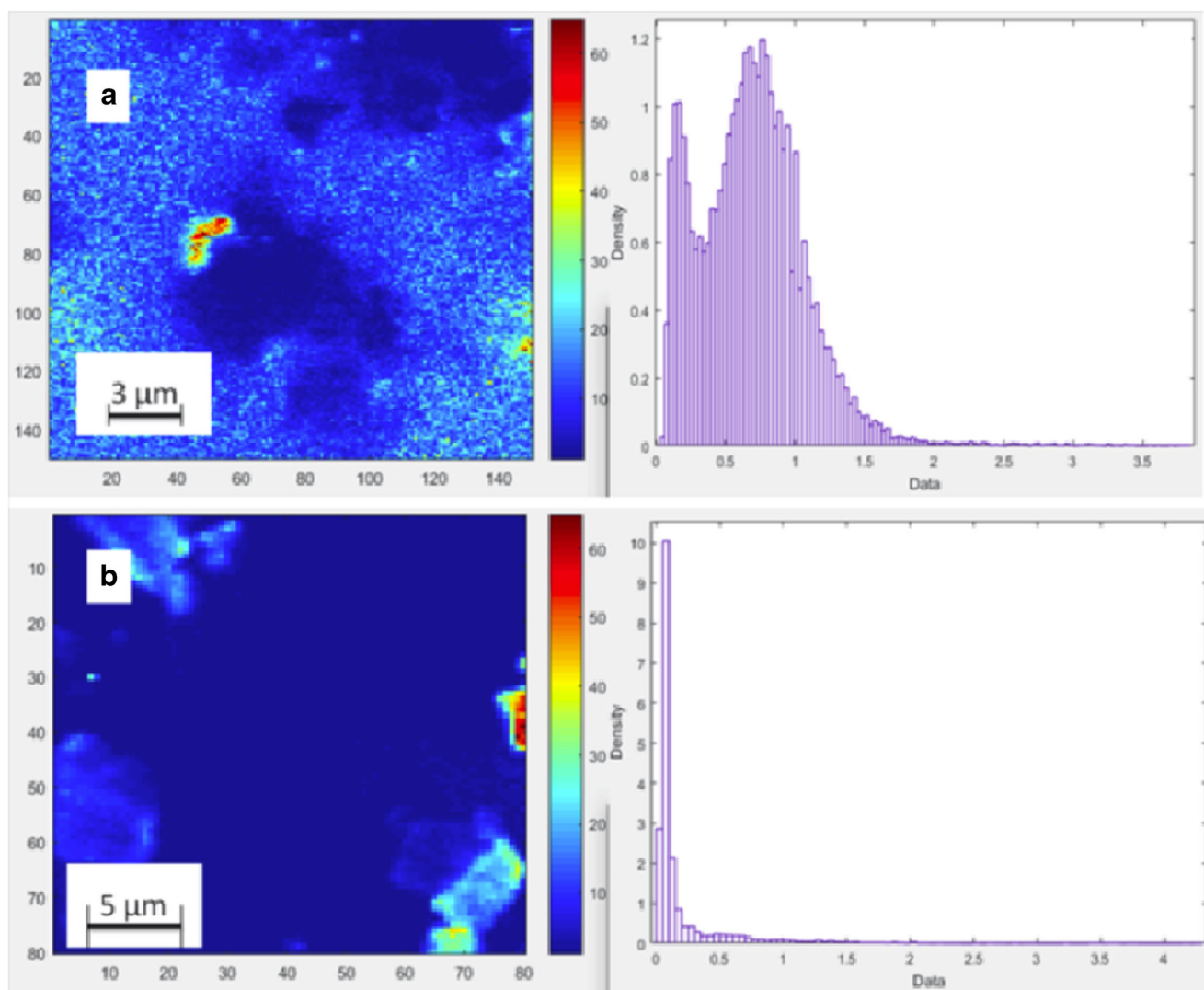


**Fig. 7** XY confocal Raman microscopy mapping of FBZ/P407 SD22 (**a**) and PM22 (**b**); their corresponding histograms are shown on the right. Scale bars indicate the intensity ratio  $I_{1591}/I_{866}$ . All the images include the number of the grid points in X and Y axis, and the corresponding bar length



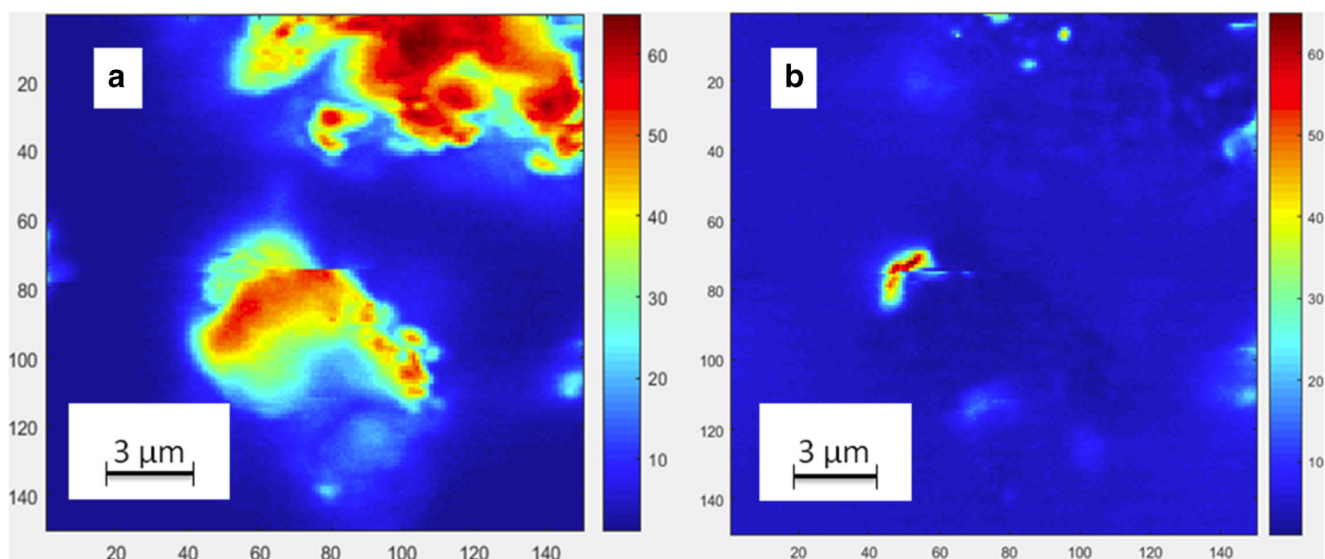


**Fig. 8** PCA reconstructed image of SD22 considering. **a** PC1. **b** PC2. All the images include the number of the grid points in X and Y axis, and the corresponding bar length

The principal component analysis (PCA) images of the samples were obtained by processing the same spectral data used to calculate the normalized  $I_{1591}/I_{866}$  2D confocal Raman mapping. In the analysis of SD22, the principal component 1 (PC1) explains almost 90% of the variance within the data set. PCA imaging allowed for the discrimination between two groups. The first group corresponds to a zone represented in blue, with a mean spectrum that corresponds to a mixture of FBZ and P407, and zones with higher score values with mainly P407 composition (Fig. 8a). When analyzing the mapping of the second principal component (PC2), which represents less than 5% of the explained variance, the image discriminates a few spots of FBZ composition at higher score values (Fig. 8b). On the other hand, in the reconstructed PM22

image, the PC1 represents also 90% of the explained variance but its reconstructed image (Fig. 9) discriminates between three groups: an extended zone in blue which corresponds to pure P407, a small transition zone in sky-blue where the mean spectra show the presence of both components, and a zone with higher score values that represents pure FBZ. On the other hand, in this case, PC2 did not provide different information from PC1.

These PCA results confirm what was previously observed with the normalized  $I_{1591}/I_{866}$  2D mapping, which indicated that the distribution of FBZ is better within the polymeric matrix in the SD in comparison to that of the PM, which could allow us to assure a better content uniformity. Additionally, from the data analysis point of view, the utilization of PCA constitutes a powerful and fast technique that does not require further data reduction nor manipulation. This structural characterization clearly explains the remarkable differences between the dissolution curves obtained for DSs and PMs, indicating also that the crystalline fraction of P407/P188 is reduced when subjected to SD processes.

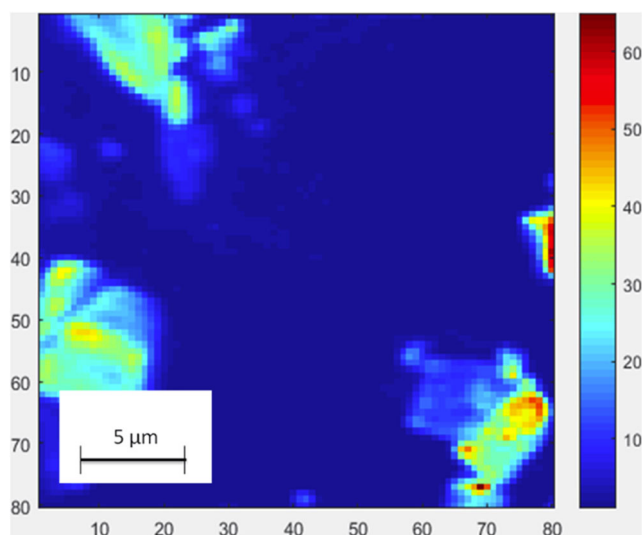


**Fig. 9** PCA reconstructed image of PM22, considering PC1. The image includes the number of the grid points in X and Y axis, and the corresponding bar length

## Conclusions

In this work, it was demonstrated the usefulness of Raman chemical imaging as a fast, powerful, and non-destructive method in pharmaceutical development.

In fact, with the aim to enhance aqueous solubility of fenbendazole, binary solid dispersions containing two different poloxamer carriers were prepared using a low-temperature fusion method. In vitro dissolution results exhibited a marked improvement when FBZ was formulated as SD. The solid state properties of these preparations were characterized by

different techniques such as X-ray powder diffraction (XRPD), Raman confocal microscopy and Fourier transform infrared spectroscopy, and SEM.

The most relevant contribution of structural characterization was to probe that the crystalline fraction of P407/P188 is reduced and FBZ is better distributed within the polymeric matrix in the SD.

We hope that this methodology can be used in the future to address similar materials contributing to the design of new drug delivery systems and could be incorporated towards the use of quality by design (QbD) approaches in pharmaceutical development.

**Acknowledgments** The authors especially thank Dario O. Weitmann, Business Coordinator BCS in BASF Argentina S.A for the Poloxamer samples, Q.F. Antonio Malanga (BIOTEFA—Instituto Polo Tecnológico de Pando, Facultad de Química, UdelaR, Uruguay) for kindly providing access to the necessary equipment, and Lourdes Martino, who edited this paper. The authors acknowledge Prof. Dr. Alejandro Ayala (Universidade Federal do Ceará, UFC, Brazil) for providing DSC and TG measurement, and Fernando Pignanelli (Facultad de Química, UdelaR, Uruguay) for the help in the implementation of PCA and the peak-to-peak computational scripts for the data analysis.

**Funding Information** This work was supported by grants from the Programa de Desarrollo de Ciencias Básicas (PEDECIBA, Uruguay), ANII (Agencia Nacional de Investigación e Innovación, Uruguay), Project ANII-EQC-X-2012-1-14 IPTP, AUGM (Asociación de Universidades del Grupo Montevideo), SECyT-UNC, CONICET, ANPCyT (Argentina).

## References

- Loftsson T, Brewster ME. Pharmaceutical applications of cyclodextrins: basic science and product development. *J Pharm Pharmacol*. 2010;62(11):1607–21. <https://doi.org/10.1111/j.2042-7158.2010.01030.x>.
- Leuner C, Dressman J. Improving drug solubility for oral delivery using solid dispersions. *Eur J Pharm Biopharm*. 2000;50(1):47–60. [https://doi.org/10.1016/S0939-6411\(00\)00076-X](https://doi.org/10.1016/S0939-6411(00)00076-X).
- Vasconcelos T, Sarmiento B, Costa P. Solid dispersions as strategy to improve oral bioavailability of poor water soluble drugs. *Drug Discov Today*. 2007;12(23):1068–75. <https://doi.org/10.1016/j.drudis.2007.09.005>.
- Brough C, Williams RO. Amorphous solid dispersions and nanocrystal technologies for poorly water-soluble drug delivery. *Int J Pharm*. 2013;453(1):157–66. <https://doi.org/10.1016/j.ijpharm.2013.05.061>.
- Vo CL-N, Park C, Lee B-J. Current trends and future perspectives of solid dispersions containing poorly water-soluble drugs. *Eur J Pharm Biopharm*. 2013;85(3):799–813. <https://doi.org/10.1016/j.ejpb.2013.09.007>.
- Mehanna MM, Motawaa AM, Samaha MW. In sight into taladafil-block copolymer binary solid dispersion: mechanistic investigation of dissolution enhancement. *Int J Pharm*. 2010;402(1):78–88. <https://doi.org/10.1016/j.ijpharm.2010.09.024>.
- Bhandari KH, Nawa M, Kim JA, Yoo BK, Woo JS, Lyoo WS, et al. Preparation, characterization and evaluation of coenzyme Q10 binary solid dispersions for enhanced solubility and dissolution. *Biol Pharm Bull*. 2007;30(6):1171–6. <https://doi.org/10.1248/bpb.30.1171>.
- U.S. Food and Drug Administration, Center for Drugs Evaluation Research (CDER), Center for Veterinary Medicine (CVM) and Office of Regulatory Affairs (ORA). Guidance for Industry: PAT - A Framework for Innovative Pharmaceutical Development. 2004. <https://www.fda.gov/downloads/Drugs/GuidanceComplianceRegulatoryInformation/Guidances/UCM070305.pdf>. Accessed 11 Dec 2017.
- Vasanthavada M, Tong W-Q, Serajuddin A. Development of solid dispersions for poorly water-soluble drugs. In: Liu R, editor. *Water insoluble-drug formulation*. 2nd ed. Boca Raton: CRC Press; 2008. p. 499–529.
- Karavas E, Georganakis M, Docoslis A, Bikiaris D. Combining SEM, TEM, and micro-Raman techniques to differentiate between the amorphous molecular level dispersions and nanodispersions of a poorly water-soluble drug within a polymer matrix. *Int J Pharm*. 2007;340(1):76–83. <https://doi.org/10.1016/j.ijpharm.2007.03.037>.
- Furuyama N, Hasegawa S, Hamaura T, Yada S, Nakagami H, Yonemochi E, et al. Evaluation of solid dispersions on a molecular level by the Raman mapping technique. *Int J Pharm*. 2008;361(1):12–8. <https://doi.org/10.1016/j.ijpharm.2008.05.009>.
- Punčochová K, Vukosavljevic B, Hanuš J, Beránek J, Windbergs M, Štěpánek F. Non-invasive insight into the release mechanisms of a poorly soluble drug from amorphous solid dispersions by confocal Raman microscopy. *Eur J Pharm Biopharm*. 2016;101:119–25. <https://doi.org/10.1016/j.ejpb.2016.02.001>.
- Schoenherr C, Haefele T, Paulus K, Francese G. Confocal Raman microscopy to probe content uniformity of a lipid based powder for inhalation: a quality by design approach. *Eur J Pharm Sci*. 2009;38(1):47–54. <https://doi.org/10.1016/j.ejps.2009.05.011>.
- Haefele T, Paulus K. Confocal raman microscopy in pharmaceutical development. In: Dieing T, Hollricher O, Toporski J, editors. *Confocal raman microscopy*. Springer series in optical sciences. Heidelberg: Springer; 2010. p. 165–202.
- Choi DS, Zhang Y-E, Tian H, Shah N, Chokshi HP. Evaluation on the drug-polymer mixing status in amorphous solid dispersions at the early stage formulation and process development. *J Pharm Innov*. 2013;8(3):163–74.
- Campbell WC. Benzimidazoles: veterinary uses. *Parasitol Today*. 1990;6(4):130–3. [https://doi.org/10.1016/0169-4758\(90\)90231-R](https://doi.org/10.1016/0169-4758(90)90231-R).
- Saunders GI, Wasmuth JD, Beech R, Laing R, Hunt M, Naghra H, et al. Characterization and comparative analysis of the complete *Haemonchus contortus*  $\beta$ -tubulin gene family and implications for benzimidazole resistance in strongylid nematodes. *Int J Parasitol*. 2013;43(6):465–75. <https://doi.org/10.1016/j.ijpara.2012.12.011>.
- Longo M, Zanoncelli S, Messina M, Scandale I, Mackenzie C, Geary T, et al. In vivo preliminary investigations of the effects of the benzimidazole anthelmintic drug flubendazole on rat embryos and fetuses. *Reprod Toxicol*. 2014;49:33–42. <https://doi.org/10.1016/j.reprotox.2014.06.009>.
- Munguía B, Michelena M, Melian E, Saldaña J, Ures X, Manta E, et al. Development of novel valerolactam-benzimidazole hybrids anthelmintic derivatives: diffusion and biotransformation studies in helminth parasites. *Exp Parasitol*. 2015;153:75–80. <https://doi.org/10.1016/j.exppara.2015.03.013>.
- Munguía B, Mendina P, Espinosa R, Lanz A, Saldaña J, Andina MJ, et al. Synthesis and anthelmintic evaluation of novel valerolactam-benzimidazole hybrids. *Lett Drug Des Discovery*. 2013;10(10):1007–14. <https://doi.org/10.2174/15701808113109990028>.
- Hennessy DR. Modifying the formulation or delivery mechanism to increase the activity of anthelmintic compounds. *Vet Parasitol*. 1997;72(3):367–90. [https://doi.org/10.1016/S0304-4017\(97\)00106-4](https://doi.org/10.1016/S0304-4017(97)00106-4).
- Vilhelmsen T, Eliassen H, Schaefer T. Effect of a melt agglomeration process on agglomerates containing solid dispersions. *Int J Pharm*. 2005;303(1):132–42. <https://doi.org/10.1016/j.ijpharm.2005.07.012>.

23. Zhai H, Li S, Andrews G, Jones D, Bell S, Walker G. Nucleation and growth in fluidised hot melt granulation. *Powder Technol.* 2009;189(2):230–7. <https://doi.org/10.1016/j.powtec.2008.04.021>.
24. Kibbe AH, American Pharmaceutical A. *Handbook of pharmaceutical excipients*. Washington, D.C.: American Pharmaceutical Association; 2000.
25. Xie F, Ji S, Cheng Z. In vitro dissolution similarity factor (f<sub>2</sub>) and in vivo bioequivalence criteria, how and when do they match? Using a BCS class II drug as a simulation example. *Eur J Pharm Sci.* 2015;66:163–72. <https://doi.org/10.1016/j.ejps.2014.10.002>.
26. *Pharmacopeia U. USP 29–NF 24*. Rockville: USP; 2005.
27. Castro SG, Bruni SS, Lanusse CE, Allemanni DA, Palma SD. Improved albendazole dissolution rate in Pluronic 188 solid dispersions. *AAPS PharmSciTech.* 2010;11(4):1518–25. <https://doi.org/10.1208/s12249-010-9517-6>.
28. Horvat AJ, Babić S, Pavlović D, Ašperger D, Pelko S, Kaštelan-Macan M, et al. Analysis, occurrence and fate of anthelmintics and their transformation products in the environment. *TrAC Trends Anal Chem.* 2012;31:61–84. <https://doi.org/10.1016/j.trac.2011.06.023>.
29. Craig DQM. The mechanisms of drug release from solid dispersions in water-soluble polymers. *Int J Pharm.* 2002;231(2):131–44. [https://doi.org/10.1016/S0378-5173\(01\)00891-2](https://doi.org/10.1016/S0378-5173(01)00891-2).
30. Eaton JW, Bateman D, Hauberg S, Wehbring R. A high-level interactive language for numerical computations. In *GNU Octave version 4.2.1*. Free Software Foundation. 2017. <https://www.gnu.org/software/octave/octave.pdf>. Accessed 11 Dec 2017.